Dedicated low-field MRI in mice

P. Choquet, E. Breton, C. Goetz, C. Marin, André Constantinesco

Dedicated low-field MRI in mice

P Choquet[1], **E Breton**[1,3], **C Goetz**[1], **C Marin**[2] **and A Constantinesco**[1,4]

[1] Laboratoire de Biomécanique, IMFS, Service de Biophysique et Médecine Nucléaire, Hôpitaux Universitaires de Strasbourg, CHU Hautepierre, 1 Avenue Molière, 67098 Strasbourg, France
[2] Service d'Anatomo-Pathologie, Hôpitaux Universitaires de Strasbourg, CHU Hautepierre, 1 Avenue Molière, 67098 Strasbourg, France

E-mail: Andre.CONSTANTINESCO@chru-strasbourg.fr

Abstract
The rationale of this work is to point out the relevance of *in vivo* MR images of mice obtained using a dedicated low-field system. For this purpose a small 0.1 T water-cooled electro-magnet and solenoidal radio frequency (RF) transmit–receive coils were used. All MR images were acquired in three-dimensional (3D) mode. An isolation cell was designed allowing easy placement of the RF coils and simple delivery of gaseous anesthesia as well as warming of the animal. Images with and without contrast agent were obtained in total acquisition times on the order of half an hour to four hours on normal mice as well as on animals bearing tumors. Typical in plane pixel dimensions range from 200 $\times$ 200 to 500 $\times$ 500 μm^2 with slice thicknesses ranging between 0.65 and 1.50 mm. This work shows that, besides light installation and low cost, dedicated low-field MR systems are suitable for small rodents imaging, opening this technique even to small research units.

1. Introduction

In vivo imaging can now be considered as a unique non-invasive tool for physiological studies, diagnosis and longitudinal follow-up of small animal disease models (rat and mouse) (Rudin and Sauter 1992, Green *et al* 2001, Ritman 2002).

Small animal imaging techniques are however limited by some aspects of the physiology of rat and mouse, their size and by the spatial, temporal, functional and molecular resolutions of the available devices. Among the armory of imaging modalities, MRI based on the ^{1}H nuclei magnetic properties in a magnetic field, offers the unique opportunity to produce images with

[3] Present address: New York University, Langone Medical Center, Department of Radiology, Center for Biomedical Imaging, 660 1st Avenue, 1st floor, New York, NY 10016, USA.
[4] Author to whom any correspondence should be addressed.

various contrasts, due to the natural ^{1}H abundance in living tissues. As examples, some of them are T_1- and T_2-dependent due to relaxation properties of tissues and can be enhanced using specific agents as gadolinium, iron oxide nanoparticles or manganese, but diffusion, angiographic and flow images can also be obtained (Hu *et al* 2001, Silva *et al* 2004, Wu *et al* 2004). Besides occasional use of clinical MR scanners (Brockmann *et al* 2006), the high spatial resolution required by the rat and mouse organ dimensions is classically achieved with magnetic fields ranging from 2.3 T up to 14 T, giving an enhanced signal to noise ratio (S/N) (Glover and Mansfield 2002, Marzola *et al* 2003, Pautler 2004, Schneider *et al* 2003). However, even at a very high magnetic field, the technique is still time consuming (ranging from 30 min to 4 h per examination for MR microscopy depending on the imaging strategies and the goal of the study (Benveniste and Blackband 2002)). Accurate physiological monitoring of the animal, as well as establishing homeostatic conditions inside the magnet, is mandatory during the whole imaging procedure to be sure that images were obtained in the best conditions for the animal and also to avoid blurring of the images. All these requirements remain difficult to achieve properly, some limits being due to physiological movements (Mai *et al* 2005).

Nevertheless, high field small animal MRI has reached the status of being a current and mature technique. Magnet and experimental setup require particular attention and investigators should consider that although it is probably the most versatile among all the imaging modalities, it is also the most complex. It requires skill and a huge experience. Finally, it is a high-cost technique along with low throughput which in turn restricts its use. These drawbacks tend currently to push MRI toward being a useful tool for second-line specialized investigations in small animal phenotype imaging (Monassier and Constantinesco 2006). Given these facts and considering the small amount of work done lowering the main magnetic field B_0, it is interesting to evaluate the performance of a low magnetic field (0.1 T) for *in vivo* small animal imaging and not to take for definitive the initial results obtained on small animals many years ago using low magnetic fields. We will present examples of MR images acquired *in vivo* on normal and pathological mice with fields of view ranging from whole body to such a small part as a tail. This last example is intended for checking limits of our system. Arguments in favor of its suitability for small rodents imaging (Breton *et al* 2005) will be discussed based on the results obtained.

2. Material

2.1. Animal procedures, anesthesia and MR contrast agent administration

Two normal adult female mice (CD1) weighing 27 g $\pm$ 3 g, one CD1 mouse (50 g) bearing subcutaneous tumor (Inserm U682, Strasbourg, France) and one SWISS nude mouse (34 g) bearing human brain glioblastoma (Transgene, Strasbourg, France) were included in this study according to the French regulations concerning small animals experimentation (authorizations A 67-482-20 and 67–104). During imaging, animals were maintained under gaseous anesthesia (isoflurane 0.5–1.5% with air) using an anesthesia mask with a bite bar in an air heated non-magnetic cylindrical Plexiglass cell designed for small animal multimodal imaging (Universal Cell for Small Animal Imaging, Minerve Équipement Vétérinaire, Esternay, France) allowing extended *in vivo* imaging acquisition (figure 1). For monitoring of vital signs, thanks to a technical pipe built inside the imaging cell, ECG was recorded using carbon ECG pads connected to an electrocardiograph (Physiogard RSM784, Bruker/ODAM, Wissembourg, France) and respiration was followed via a pressure sensor (RX110, Biopac Systems Inc., Goleta, CA, USA) connected to a pressure transducer (Minerve Équipement Vétérinaire,

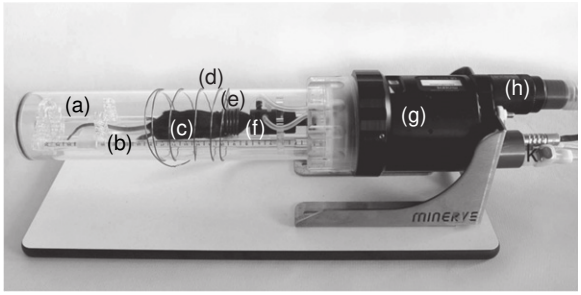

Figure 1. The universal cell for small animal imaging in the configuration for use in the 0.1 T magnet. (a) Plexiglass tube aimed at complete insulation of the animal, (b) bed and rules, (c) animal, (d) matching coil, (e) transmit–receive MR coil tuned at 4.26 MHz, (f) anesthesia mask with bite bar, (g) cell body, (h) anesthesia gas circulation, (k) electrical connections and air circulation used by the heating system.

Esternay, France). When needed and for improving T_1 weighted contrast images, 1 ml of gadoteric acid (Dotarem 0.5 mmol ml^{-1}, Guerbet, France) diluted four times in physiological solution was administered intraperitoneally (i.p.).

2.2. Low-field dedicated MR imager

Dedicated low-field MR imagers used in this work were previously developed for hand, wrist and finger imaging (Gries *et al* 1991, Arbogast-Ravier *et al* 1995). B_0 is generated by a 0.1 T water-cooled resistive magnet (electrical consumption 3230 W, power supply class 10 ppm, water flow 3 l min^{-1}) weighting 800 kg and whose dimensions are 70 cm $\times$ 70 cm wide and 1.10 m height (Bouhnik SAS, Velizy-Villacoublay, France). The magnet used has an 18 cm air gap. The field homogeneity in a cylinder of 60 mm diameter and 100 mm length at the center of the magnet is $\pm$5 ppm. The encoding gradients have a maximum amplitude of 20 mT m^{-1} which can be reached in less than 0.5 ms (figure 2). The maximal temporal drift during 4 h of the Larmor frequency was measured at 50 Hz.

The orientation of the magnetic field allows the use of solenoidal coils specifically designed for small laboratory animals in order to optimize the filling factor and for offering a proper homogeneity of the RF pulse with a measured quality factor ranging between 57 (for the smallest one of 4 mm internal diameter, used for tail imaging) and 340 (for the larger one of 55 mm internal diameter), whatever the load due to their small size and the low working frequency (table 1). The RF transmit–receive coils are tuned around 4.26 MHz, which is the proton resonance frequency at 0.1 T, and the value of B_0 can be modified a little around this value to match the Larmor frequency. The use of the imaging cell allows a pickup loop to be slid around the cylindrical Plexiglass tube for inductive coupling to preamplifier (figure 1). MRI acquisition sequences were developed on a SMIS console (MR Research Systems Ltd, Guildford, United Kingdom). A large range of classic MRI sequences (spin echo, gradient echo ones: FLASH, FAST, FISP, CE-FAST) giving proton density, T_1, T_2 or T_2^* contrasts were implemented. For the purpose of this work, all the sequences used were fast gradient echo imaging sequences and were developed in 3D mode offering a better S/N ratio than two-dimensional multi-slice acquisitions at the expense of an increased imaging time (Johnson *et al* 1987).

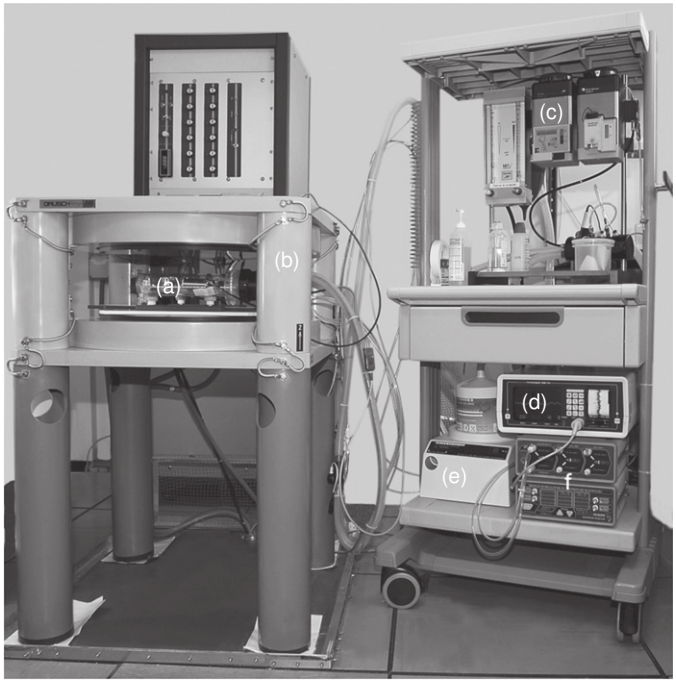

Figure 2. The 0.1 T magnet with the gaseous anesthesia apparatus beside. (a) The universal cell with the animal placed inside the magnet, (b) 0.1 T resistive magnet, (c) anesthesia system, (d) ECG monitor, (e) filter system to trap scavenging anesthetic gas, (f) heating system: control unit and air circulation pump.

Table 1. Characteristics of the solenoidal coils used in this study, from the smallest one to the largest. The name by which they are listed refers to their use and is recalled in each figure caption.

Coil name	Internal diameter (mm)	Length (mm)	Wire diameter (mm)	Number of turns	Quality factor
Tail	4.0	9	1.0	8	80
Head	8.2	14	2.4	5	200
Whole body 1	17.5	30	2.0	5	190
Whole body 2	55.0	56	2.0	6	340

S/N was measured using ImageJ (Abramoff *et al* 2004) by the ratio of the mean pixel value measured in a region of interest in the animal, to the standard deviation of the pixel value measured in a background region of interest.

2.3. Tail histology

After completion of the MRI procedure and euthanasia of the mouse, the tail was prepared for light microscopic examination. After fixation in 10% neutral buffered formalin and sufficient decalcification, the tail was cut in 3 mm length segments and embedded in paraffin. Then 4 μm thickness transversal sections were stained with hematoxylin and eosin.

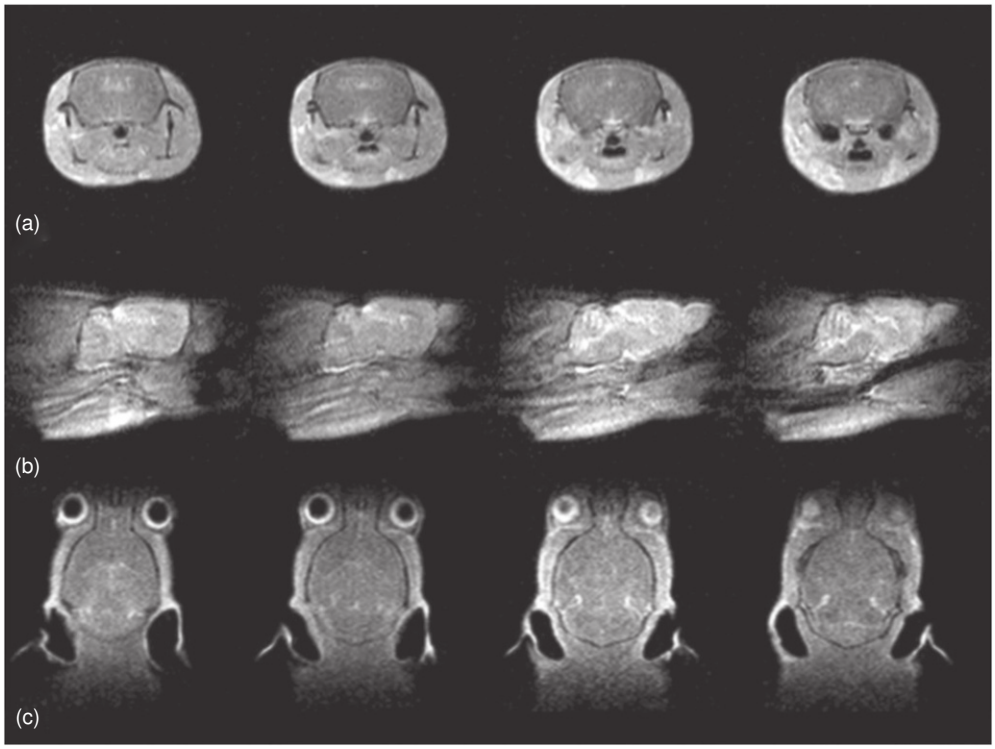

Figure 3. Transverse (a), sagittal (b) and frontal (c) slices of a mouse head. Head coil. FAST sequence (TE/TR = 9/100 ms, FA 80°, BW 16.7 kHz, matrix 128 × 96 × 32 reconstructed in 128 × 128 × 32, field of view 26 mm, slab thickness 20 mm, acquisition time in one direction 4h07 for 32 slices in 3D mode) after i.p. administration of gadoteric acid. Reconstructed voxel size: 203 × 203 μm^2 with a slice thickness of 625 μm.

3. Results

During all experiments, recorded ECG and respiratory signals remained steady whatever the duration of acquisition.

Figure 3 shows T_1 weighted series of images of the mouse head in the three basic reference planes. The adjunct of a gadolinated contrast agent allows for an enhancement of S/N in these acquisition conditions. On the transverse images (figure 3(a)), the ventricles, lateral and third, are easily observed, the fourth being visible on the coronal images (figure 3(c)). The more precise delineation of normal brain structures is seen in the sagittal plane (figure 3(b)): from caudal to rostral direction, the territories corresponding to cerebellum, brain stem, thalamus, corpus callosum, pituitary gland and olfactory bulbs could be identified. The consequence of the small volume of the voxels is clearly the increased acquisition time required to achieve an acceptable S/N, which is in this case equal to 32.

With a larger field of view, figure 4 shows organs at the level of thorax and of cranial part of the abdomen. The use of the i.p. route for contrast agent administration is responsible for the enhanced signal in abdominal cavity. The S/N was measured at 43 by taking the liver for signal reference.

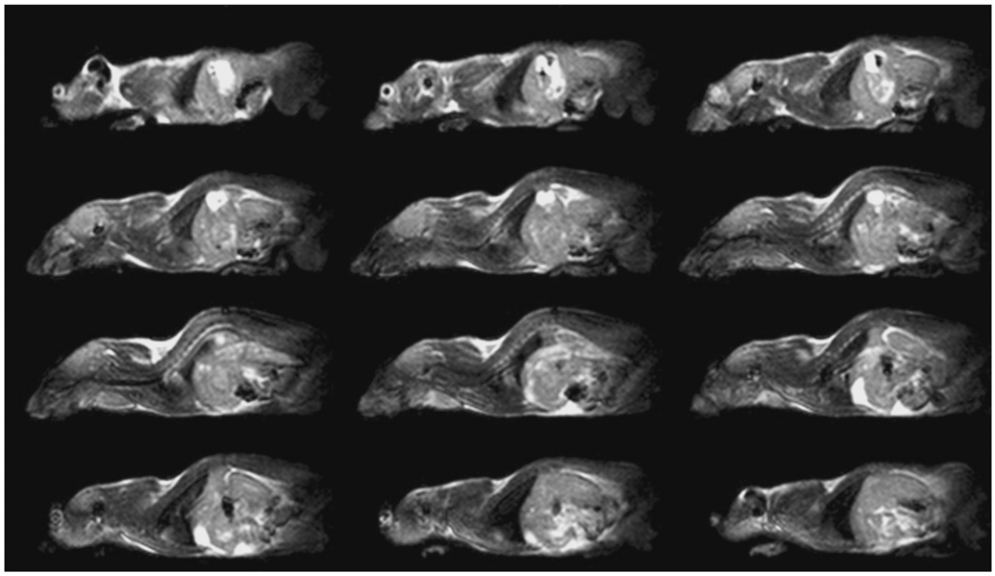

Figure 4. Twelve consecutive slices in the sagittal plane encompassing the head, thorax and cranial part of the abdomen of a living mouse. Whole body 1 coil. FISP sequence (TE/TR = 9.8/21 ms, FA 70°, BW 20 kHz, matrix 192 × 96 × 32 reconstructed in 256 × 128 × 32, field of view 110 mm, slab thickness 34 mm, acquisition time 33 min for 30 slices in 3D mode). Reconstructed voxel size: 430 × 430 μm^2 with a slice thickness of 1.06 mm.

In figure 5, the large subcutaneous tumor gives an overall higher signal than the soft tissue around. The content is highly heterogenous, with some calcification occurring (from microCT data, not shown). Although the acquisition time is kept short with a lower S/N ratio (22 between tumor and background), the tumor is easily visible.

Figure 6 shows an example of a tumor model of the brain. Taking a low spatial resolution (the biggest voxel volume presented in this paper) and a short acquisition time, we obtain a S/N of 43 between tumor (measured volume of 105 mm^3 by methods described by Israel-Jost *et al* (2008)) and background. The lack of the blood brain barrier relative to the normal brain tissue is responsible for the uptake of the contrast agent and so the high signal obtained in the tumor.

The voxel size of the acquisition shown in figure 7 is at the limit of the microscopic domain as usually defined: 100 μm in one dimension. The corresponding histological slice enables the recognition of the main structures of the tail.

4. Discussion

We demonstrate that given the use of well-designed coils and of gradients of high amplitude value, we are able to obtain meaningful MR images of mice *in vivo* at 0.1 T, at the price of a long acquisition time. Both normal and pathological structures are sufficiently outlined to allow for anatomical description and diagnosis. We are able to achieve *in vivo* voxels as small as 100 × 100 × 750 μm^3: the image of the tail, thanks to the gain in the S/N ratio when using smallest coils, shows that we can obtain not only signal but also contrast

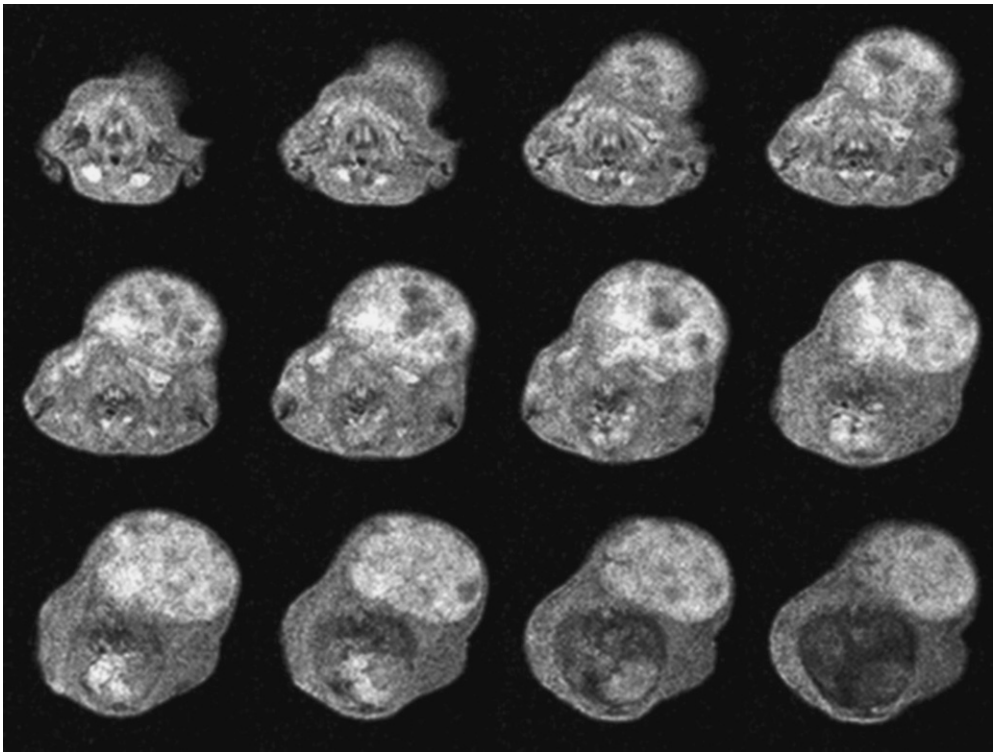

Figure 5. Twelve consecutive slices (cranio-caudal direction from top-left to bottom-right images) in the transverse plane through a spontaneous sub-cutaneous tumor, developing on the neck. Whole body 2 coil. FLASH sequence (TE/TR = 10/21 ms, FA 70°, BW 16.7 kHz, matrix 128 × 96 × 24 reconstructed in 128 × 128 × 32, field of view 44 mm, slab thickness 48 mm, acquisition time 30 min for 24 slices in 3D mode). Reconstructed voxel size: 344 × 344 μm^2 with a slice thickness of 1.5 mm.

and distinguish between tissues as demonstrated by the corresponding histology slice, given beside as illustration.

Early rodent MR imaging works (Hansen *et al* 1980, Herfkens *et al* 1981, 1983) were done on a clinical system operating at 0.35 T, making use of available state-of-the-art systems at this time: it is not meaningful to compare their results with those obtained nowadays on up-to-date systems as well as to base the judgment of low-field MRI only on these preliminary results. In 1986 and 1987, Johnson *et al* (1986, 1987) proposed the use of a clinical scanner working at 1.5 T taking advantage of modified gradients coils to achieve a voxel size of 115 × 115 × 1000 μm^3 in rats. Afterward, small animal MRI was exclusively done on specialized MR systems, working at higher magnetic fields, except for very few works. In the case of the mouse, whole body images were obtained at 0.15 T (Henkelman *et al* 1987), and at 0.35 T to look at intra-organ tumors (Fiel and Button 1990, Button *et al* 1990), *ex vivo* images on newborns were acquired using a dedicated system working at 0.21 T (Wright *et al* 2002) and *in vivo* brain and whole body images using a permanent magnet working at 1 T (Shirai *et al* 2005, Inoue *et al* 2006). On the rat, hepatic metastases were observed at 0.6 T (Chen *et al* 1989), brain images were done at 0.35 T, correlated with histology (Fiel *et al* 1991) and at 0.2 T (Yamada *et al* 1995). In

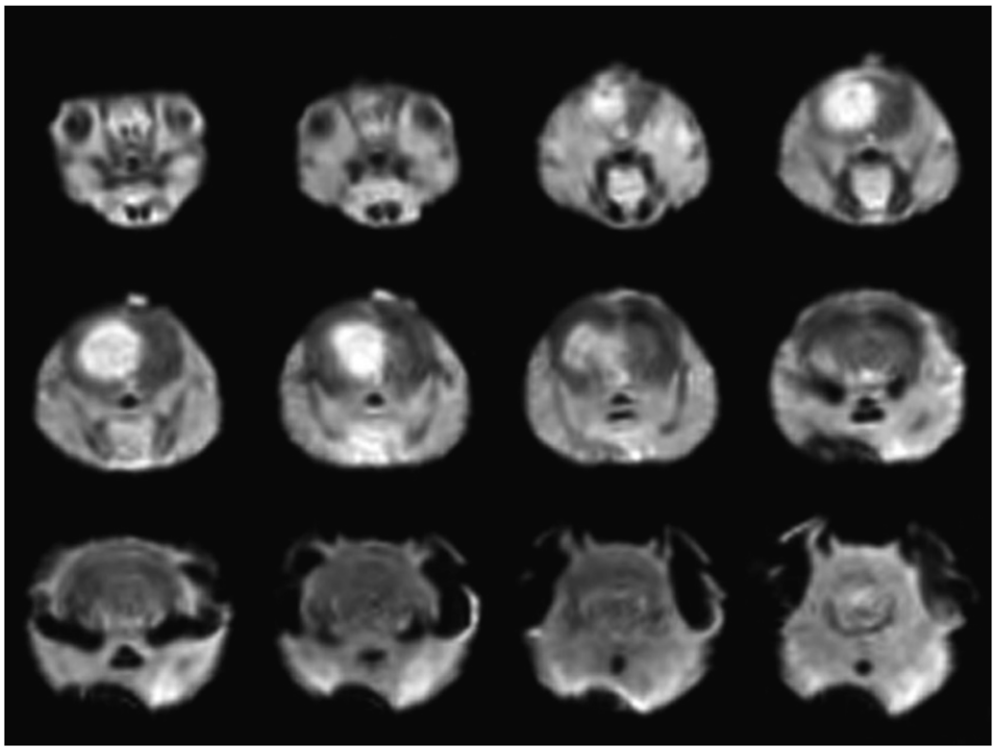

Figure 6. Twelve consecutive slices in the transverse plane (rostro-caudal direction from top-left to bottom-right images) through the head of a mouse bearing a human glioblastoma. Head coil. FAST sequence (TE/TR = 8.5/120 ms, FA 80°, BW 16.7 kHz, matrix 64 × 64 × 32, field of view 26 mm, slab thickness 40 mm, acquisition time 41 min for 32 slices in 3D mode) after i.p. administration of gadoteric acid. Reconstructed voxel size: 406 × 406 μm^2 with a slice thickness of 1.25 mm.

the last place, we can cite more niche applications like assessing with ^{19}F partial pressure of oxygen in rat tissues at 0.14 T (Pratt *et al* 1997) and MRI of laser polarized ^{3}He in rat lungs at 88 mT (Suchanek *et al* 2005). Recently, the engineering process for building low-field electro-magnets aimed at small animal imaging was reported (Gilbert *et al* 2006).

4.1. 'Low' versus 'high' magnetic field

It is necessary to call attention to the non-obvious designation of the working field value for a given magnet. The distinction made between 'low' and 'high' magnetic fields is especially subjective: for human applications a high field is about 1.5 T and above (3 T are now designated as ultrahigh field), while for animals, a 2 T system is at present regarded as a low-field system (Natt *et al* 2002). This distinction is arbitrary and not scientifically based, leading for some users to an incorrect association between low field value and low achievable spatial resolution. What is incontrovertible is that the magnetic field value alone is not the only characteristic to take into account when evaluating a MRI system, as improvements are easily seen in commercial systems although the magnetic field value is kept constant (for example the 1.5 T systems sold for near 20 y). In the same way, the denomination high-quality image is not very informative: what is high quality one day often becomes low quality some years later.

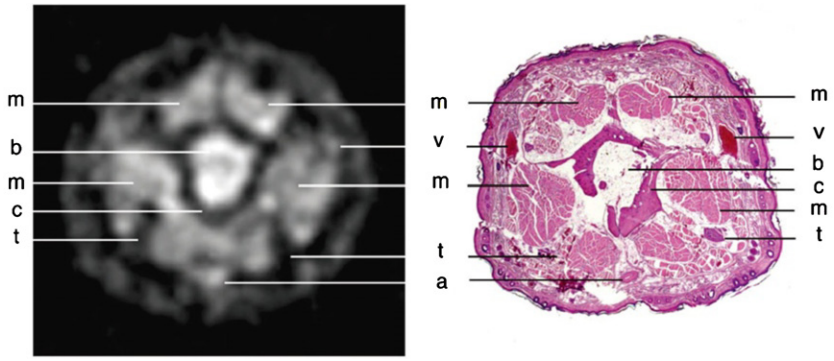

Figure 7. Left: transverse slice through the tail of a mouse, acquired *in vivo*. Tail coil. FAST sequence (TE/TR = 16/100 ms, FA 80°, BW 5 kHz, matrix 64 × 64 × 26 reconstructed in 64 × 64 × 32, field of view 6.4 mm, slab thickness 24 mm, acquisition time 1h30 for 26 slices in 3D mode). Reconstructed voxel size: 100 × 100 μm^2 with a slice thickness of 750 μm. Right: the homologous histological slice. (a) Artery, (b) bone marrow, (c) cortical bone, (m) muscle, (t) tendon, (v) vein.

(This figure is in colour only in the electronic version)

4.2. Spatial resolution

On a theoretical basis, there is no relationship between the B_0 value and the voxel size. Strictly speaking, the voxel size depends only on the amplitude and application time of the gradients and the value of B_0 is not involved in the calculation:

$$d = \frac{2\pi\,\Delta\nu}{\gamma G N},$$

where d is the dimension of the voxel in the direction in which a magnetic field gradient G is applied, γ is the gyromagnetic ratio, $\Delta\nu$ is the bandwidth of the received signal and N is the number of pixels in a line of picture matrix (Johnson *et al* 1986). A practical limit is set by the homogeneity of the magnet and susceptibility differences measured by T_2^*, a shorter value being much difficult to achieve as B_0 increases (Glover and Mansfield 2002).

However, the major limiting factor for acquiring small voxels remains the S/N ratio, depending mainly on the B_0 value (Callaghan 1982). It governs the ability to see small objects and distinguish between them, which is the definition of the spatial resolution of an instrument. It shall be noted that there is often confusion nowadays between dimensions of the voxel (defined by the MRI system and acquisition parameters) and spatial resolution (which must be measured). Complete evaluation of resolution achievable by a given system involves both aspects, bringing together gradients amplitude and B_0 value, and leads to the belief that it is not possible to image small objects at low magnetic field values. In fact it is not true, as long as the issue of S/N is addressed.

The discussion on spatial resolution calls for two remarks.

- Dealing with the voxel size and technological comparison, it is important not to lose sight of the most important thing: giving a response to the biological question. It may or may not need a high field value of B_0. But what remains is the question of interest: are the images, whatever their quality, able to give an unequivocal response? For instance, on the cerebral tumor model (figure 6), we could easily detect the tumor and calculate a volume

from the images (Israel-Jost *et al* 2008), of interest for a follow-up during a treatment trial.

- it is widely assumed that the smallest is the best. However, there are few arguments in many cases about the real need for improved resolution. The highest resolution is not always a requirement; functional imaging (by use of radioisotopes in human beings and animals, or optical probes in animals) is affected in general by a 'poor' spatial resolution while giving significant information. All answers do not lie in the size of voxels.

4.3. Pro: less artifacts, con: acquisition time and S/N ratio

It is well known that many MRI artifacts (especially susceptibility ones) are field dependent, and so it is more simple to work at low field. The major but almost only disadvantage (if we are not considering proton spectroscopic information) is the dramatic reduction in the S/N ratio. The only way to limit this effect is by increasing averages and so the acquisition time as well as making systematic use of 3D mode acquisition sequences. Due to the signal dependence in B_0 on the order of the 7/4th power (Hoult and Lauterbur 1979), and in comparison with the standard B_0 value for current commercial small animal imaging systems (above 4.7 T), achieving the same voxel dimensions while retrieving the same S/N is not realistic: there is theoretically more or less a two to three orders of magnitude difference. What is more, the multiplication of the acquisition time leads only to the multiplication of the S/N ratio by the square root of the same factor. Imaging time at low field is longer than those at higher fields, given also the exclusive use of 3D acquisition sequences we made. But the difference is not as large as the ratio between B_0 values in comparison to the results: from 30 min to 4 h per scan at high fields (Benveniste and Blackband 2002). Of course, some dynamic studies of rapid physiological processes are hampered by these longer acquisition times.

Improvements remain achievable through the use of cooled RF coils. A gain in S/N of about 2 to 3 is expected (Hoult and Richards 1976) using either copper (Wright *et al* 2000) or high-temperature supraconductive coils (Ma *et al* 2003). As the noise from the coil itself is mainly predominant at low frequencies over the noise from the sample, cooling the coil is very effective at low field even with coils of large dimensions.

4.4. Management of the animal

The main problem of lengthening acquisition is when *in vivo* imaging is involved, anesthesia is required during a long period of time as well as the necessity to keep the animal in conditions of homeostasis. It is well known that especially in mice the temperature is a critical parameter. Thanks to the use of an innovative imaging cell, we can maintain the animal temperature constant, while keeping it under gaseous anesthesia and monitoring some physiological parameters. Images of normality (figures 3 and 4) shown in the present paper were obtained on two animals only, e.g. the same animal was used in different acquisition protocols, on different days, during which it could stay in the magnet inside the cell as long as 11h30, waking up at the end of the experiment. The open configuration (on three sides) of the magnet also allows for a direct visual control of the animal, and for a quick intervention if needed.

4.5. Interest in multimodalities systems

In functional imaging, coregistration with anatomical landmarks is really an added value. It could be provided by microCT, but for obtaining soft tissue contrast without administration

of compounds, MRI could be a choice. The actual development of multimodality imaging in human beings, but more importantly in small animal imaging, poses two questions:

- first dealing with the relative voxel sizes achieved by each of the combined technology: as it does not make sense to merge data whose spatial resolutions are on the order of 1 mm^3 (in SPECT, PET or optical imaging) with ones of the order of 0.001 mm^3 (for an isotropic 100 microns side cubic voxel in microscopic MRI), e.g. as MRI microscopic resolution is not meaningful, low-field MRI could be used, with the advantage of simplicity;
- in such systems, the goal is to limit registration problems by putting all modalities on the same mechanical line, which requires that the different systems shall not interfere with each other. The fringe field of the electro-magnet used in this study is very close to the magnet, and allows for use of systems sensitive to magnetic fields in the vicinity of the MR magnets as shown in figure 2. This is true for anesthesia systems but potentially also for SPECT, PET or optical systems based on the use of photomultipliers. These two points are undoubtedly in favor of the low field for the MR part in hybrid systems, as we demonstrated with SPECT (Goetz *et al* 2008).

4.6. Safety of MRI

It is widely accepted that MRI has no or little side effects. One well-known possible source of danger relies on the power of the RF pulses, but these remain under control. Possible biological effects of high static magnetic field were recently stated (Valiron *et al* 2005) but further studies to understand and demonstrate these adverse effects are needed. No such problems were described at field lower than 5 T.

4.7. Costs

Of course the purchase of a full system, like the one used in this paper, is far cheaper than high-field ones, keeping also in mind that due to its weight (less than 1 ton) and size, there is no special requirements for the room in which it takes place. A small surface (less than 10 m^2 in our case, including the anesthesia device) of a common laboratory room could be used without any dedicated layout. If needed, a small Faraday cage could be constructed around the magnet itself. In common use, the system described based on an electro-magnet only uses water and electricity with low power requirements, can be switched off during inactivity periods and does not present extensive costs. A complete evaluation of the total costs of this system could be found in Breton *et al* (2008).

5. Conclusion

Taking into account the results reported here, we believe that there is a place beside high-field systems for what could be called a benchtop MRI, not designed to solve all questions but to do basic work on a daily basis and with an easy setup and use. Moreover, low magnetic field use in MRI has recently found some niche application thanks to the development of polarization procedures (Suchanek *et al* 2005, Goldman *et al* 2005, Adams *et al* 2009), in which the relationship between B_0 and S/N is not straightforward. In these applications, the advantage of using a 0.1 T field is based on its ability to make proton anatomical images as well for registration with functional images obtained with polarized species. Advantages of this low-field dedicated MRI system do not only lie in its low cost or its small size, but also in its ability to fulfill the requirements related to small animal imaging in terms of diagnosis and follow-up. Total examination times are comparable to high and very high field systems at the

price of a bigger voxel size but with an increased ease of experimentation. This last point is clearly important in small animal imaging. Further work will support the use of this device in pathological cases, as well as registration with other imaging modalities.

Low-field dedicated MRI systems adapted to small rodents will certainly find a particular place in the armory of molecular imaging, and undoubtedly in hybrid systems. Their light installation and low investment will allow the spread of the MRI technique to many research units.

Acknowledgments

We are grateful to General Electric Healthcare and the Région Alsace for their grant for the fellowship of E Breton, and MINERVE Équipement Vétérinaire for collaborative work on the universal imaging cell. R Rooke, P Erbs and J Kintz (Transgene, Strasbourg) as well as C Domon and J N Freund (Inserm U682, Strasbourg) helped us by providing pathological mice. C Walter and D Vetter (HUS, Strasbourg) gave us technical advice. We also wish to thank C Healy and P Berthault for careful reading of the manuscript, and J M Franconi and S Blackband for useful exchanges. Finally, a very special warm thanks to the unknown reviewers who helped us to make an appropriate demonstration.

References

Abramoff M D, Magelhaes P J and Ram S J 2004 Image processing with image *J. Biophotonics Int.* **11** 36–42

Adams R W, Aguilar J A, Atkinson K D, Cowley M J, Elliott P I, Duckett S B, Green G G, Khazal I G, López-Serrano J and Williamson D C 2009 Reversible interactions with para-hydrogen enhance NMR sensitivity by polarization transfer *Science* **323** 1708–11

Arbogast-Ravier S, Xu F, Choquet P, Brunot B and Constantinesco A 1995 Dedicated low field MRI: a promising low-cost technique *Med. Biol. Eng. Comput.* **33** 735–9

Benveniste H and Blackband S 2002 MR microscopy and high-resolution small animal MRI: applications in neuroscience research *Prog. Neurobiol.* **67** 393–420

Breton E, Goetz C, Choquet P and Constantinesco A 2005 Low field MRI in mouse *Mol. Imag.* **4** S181

Breton E, Goetz C, Choquet P and Constantinesco A 2008 Low field magnetic resonance in rat *in vivo IRBM* **29** 366–74

Brockmann M A, Ulmer S, Leppert J, Nadrowitz R, Wuestenberg R, Nolte I, Petersen D, Groden C, Giese A and Gottschalk S 2006 Analysis of mouse brain using a clinical 1.5 T scanner and a standard small loop surface coil *Brain Res.* **1068** 138–42

Button T M, Fiel R J, Goldrosen M and Paolini N 1990 Small animal MRI at 0.35 Tesla: growth and morphology of intra-organ murine tumors *Magn. Reson. Imag.* **8** 505–9

Callaghan P T 1982 *Principles of Nuclear Magnetic Resonance Microscopy* (New York: Oxford University Press)

Chen M C, Tsang Y M, Stark D D, Weissleder R, Saini S, Brandhorst J, White D L, Engelstad B L and Ferrucci J T 1989 Hepatic metastases: rat models for imaging research *Magn. Reson. Imag.* **7** 1–8

Fiel R J, Alleto J J, Severin C M, Nickerson P A, Acara M A and Pentney R J 1991 MR imaging of normal rat brain at 0.35 T and correlated histology *J. Magn. Reson. Imag.* **1** 651–6

Fiel R J and Button T M 1990 Magnetic resonance imaging of small laboratory animal *Lab. Anim. Sci.* **40** 215–6

Gilbert K M, Dalrymple B, Handler W B, Scholl T J and Chronik B A 2006 Fabrication of low-field water-cooled resistive magnets for small animal magnetic resonance imaging *Concepts Magn. Reson.* B **29** 168–75

Glover P and Mansfield P 2002 Limits to magnetic resonance microscopy *Rep. Prog. Phys.* **65** 1489–511

Goetz C, Breton E, Choquet P, Israel-Jost V and Constantinesco A 2008 SPECT low-field MRI system for small-animal imaging *J. Nucl. Med.* **49** 88–93

Goldman M, Johannesson H, Axelsson O and Karlsson M 2005 Hyperpolarization of 13C through order transfer from parahydrogen: a new contrast agent for MRI *Magn. Reson. Imag.* **23** 153–7

Green M V, Seidel J, Vaquero J J, Jagoda E, Lee I and Eckelman W C 2001 High resolution PET, SPECT and projection imaging in small animals *Comput. Med. Imaging Graph.* **25** 79–86

Gries P, Constantinesco A, Brunot B and Facello A 1991 MR imaging of hand and wrist with a dedicated 0.1 T low field imaging system *Magn. Reson. Imag.* **9** 949–53

Hansen G *et al* 1980 *In vivo* imaging of the rat anatomy with nuclear magnetic resonance *Radiology* **136** 695–700

Henkelman R M, Van Heteren J G and Bronskill M J 1987 Small animal imaging with a clinical magnetic resonance imager *Magn. Reson. Med.* **4** 61–6

Herfkens R *et al* 1981 Nuclear magnetic resonance imaging of the abnormal live rat and correlations with tissue characteristics *Radiology* **141** 211–18

Herfkens R J, Sievers R, Kaufman L, Sheldon P E, Ortendahl D A, Lipton M J, Crooks L E and Higgins C B 1983 Nuclear magnetic resonance imaging of the infarcted muscle: a rat model *Radiology* **147** 761–4

Hoult D I and Lauterbur P C 1979 The sensitivity of the zeugmatographic experiment involving human samples *J. Magn. Reson.* **34** 425–33

Hoult D I and Richards R E 1976 The signal-to-noise ratio of the nuclear magnetic resonance experiment *J. Magn. Reson.* **24** 71–85

Hu C, Pautler G, MacGowan A and Koretsky A P 2001 Manganese-enhanced MRI of mouse heart during changes in inotropy *Magn. Reson. Med.* **46** 884–90

Inoue Y, Nomura Y, Haishi T, Yoshikawa K, Seki T, Tsukiyama-Kohara K, Kai C, Okubo T and Ohtomo K 2006 Imaging living mice a 1-T compact MRI system *J. Magn. Reson. Imag.* **24** 901–7

Israel-Jost V, Breton E, Angelini E D, Choquet P, Bloch I and Constantinesco A 2008 Vectorial multi-phase mouse brain tumor segmentation in T1-T2 MRI *Proc. 5th IEEE Int. Symp. on Biomedical Imaging: From Nano to Macro, ISBI* pp 5–8

Johnson G A, Thompson M B, Gewalt S L and Hayes C E 1986 Nuclear magnetic resonance imaging at microscopic resolution *J. Magn. Reson.* **68** 129–37

Johnson G A, Thompson M B and Drayer B P 1987 Three-dimensional MRI microscopy of the normal rat brain *Magn. Reson. Med.* **4** 351–65

Ma Q Y *et al* 2003 Superconducting RF coils for clinical MR imaging at low field *Acad. Radiol.* **10** 978–87

Mai W, Badea C T, Hedlung C T and Johnson G A 2005 Effects of breathing and cardiac motion on spatial resolution in the microcopic imaging of rodents *Magn. Reson. Med.* **53** 858–65

Marzola P, Osculati F and Sbarbati A 2003 High field MRI in preclinical research *Eur. J. Radiol.* **48** 165–70

Monassier L and Constantinesco A 2006 Cardiovascular disorders: insights into *in vivo* cardiovascular phenotyping *Standards of Mouse Model Phenotyping* ed M Hrabé de Angelis, P Chambon and S Brown (Weinheim: Wiley-VCH) pp 177–200

Natt O, Watanabe T, Boretius S, Radulovic J, Frahm J and Michaelis T 2002 High-resolution 3D MRI of mouse brain reveals small cerebral structures *in vivo J. Neurosci. Methods* **120** 203–9

Pautler R 2004 Mouse MRI: concepts and applications in physiology *Physiology* **19** 168–75

Pratt R G, Zheng J, Stewart B K, Shiferaw Y, McGoron A J, Samaratunga R C and Thomas S R 1997 Application of a 3D volume ^{19}F MR imaging protocol for mapping oxygen tension (pO_2) in perfluorocarbons at low field *Magn. Reson. Med.* **37** 307–13

Ritman E L 2002 Molecular imaging in small animals-roles for micro-CT *J. Cell Biochem.* **39** 116–24

Rudin M and Sauter A 1992 *In vivo* NMR in pharmaceutical research *Magn. Reson. Imaging* **10** 723–31

Schneider J E, Cassidy P J, Lygate C, Tyler D J, Wiesmann F, Grieve S M, Hulbert K, Clarke K and Neubauer S 2003 Fast, high resolution *in vivo* cine magnetic resonance imaging in normal and failing mouse hearts on a vertical 11.7 T system *J. Magn. Reson. Imag.* **18** 691–701

Shirai T, Haishi T, Utsuzawa S, Matsuda Y and Kose K 2005 Development of a compact mouse MRI using a yokeless permanent magnet *Magn. Reson. Med. Sci.* **4** 137–43

Silva A C, Lee J H, Aoki I and Koretsky A P 2004 Manganese-enhanced magnetic resonance imaging (MEMRI): methodological and practical considerations *NMR Biomed.* **17** 532–43

Suchanek M, Cieslar K, Palasz T, Suchanek K, Dohnalik T and Olejniczak Z 2005 Magnetic resonance imaging at low magnetic field using hyperpolarized 3He gas *Acta Phys. Pol.* A **107** 491–505

Valiron O, Peris L, Rikken G, Schweitzer A, Saoudi Y, Remy C and Job D 2005 Cellular disorders induced by high magnetic fields *J. Magn. Reson. Imag.* **22** 334–40

Wright A C, Song H K and Wehrli F W 2000 *In vivo* MR micro imaging with conventional radiofrequency coils cooled to 77 K *Magn. Res. Med.* **43** 163–9

Wright S M, Brown D G, Porter J R, Spence D C, Esparza E, Cole D C and Huson F R 2002 A desktop magnetic resonance imaging system *MAGMA* **13** 177–85

Wu E X, Tang H, Wong K K and Wang J 2004 Mapping cyclic change of regional myocardial blood volume using steady-state susceptibility effect of iron oxide nanoparticles *J. Magn. Reson. Imag.* **19** 50–8

Yamada K, Miyahara K, Sato M, Hirose T, Yasugi Y, Matsuda Y and Furuhama K 1995 Optimizing technical conditions for magnetic resonance imaging of the rat brain and abdomen in a low magnetic field *Vet. Radiol. Ultrasound* **36** 523–7